phys. stat. sol. (a) **188**, No. 4, 1383–1392 (2001)

Towards a Complete Many-Body Description: Optical Response of Real Surfaces

F. BECHSTEDT[1]), W.G. SCHMIDT, and P.H. HAHN

Institut für Festkörpertheorie und Theoretische Optik, Friedrich-Schiller-Universität, Max-Wien-Platz 1, D-07743 Jena, Germany

(Received July 5, 2001; in revised form August 13, 2001; accepted August 31, 2001)

Subject classification: 71.15.–m; 71.35.–y; 73.20.At; 78.68.+m; S5.11, S7.11

We demonstrate the potential of recently developed total-energy and electronic-structure methods for the calculation of optical properties of real surfaces. We show that many-body effects such as quasiparticle shifts and electron–hole interaction can now fully be taken into account. As a prototypical property the optical reflectance anisotropy is discussed. Surface examples are large stoichiometry-dependent reconstructions of InP(001) and the hydrogen-passivated Si(110) face.

1. Introduction

Surface reflectance spectroscopies in the visible to near-UV spectral range have successfully been used for monitoring surfaces during film growth by molecular beam epitaxy and metalorganic vapour phase epitaxy as well as for exploring static surface geometries [1]. These surface sensitive techniques include among others spectroscopic ellipsometry, surface photoabsorption, and reflectance anisotropy spectroscopy (RAS), also known as reflectance difference spectroscopy (RDS) [2]. RAS is now frequently used to obtain information about the atomic structure of surfaces in various environments [3]. However, since the method gives only indirect information, a careful theoretical modelling is required [4].

Nowadays such a theoretical treatment starts usually from a parameter-free description of the system by means of the density functional theory (DFT) [5] in the local density approximation (LDA) [6]. Advanced numerical techiques for the total-energy minimization together with powerful supercomputers allow for the determination of the stoichiometry-dependent surface phases and their atomic geometries with a high accuracy even for very large surface unit cells [7, 8]. The eigenvalues and eigenfunctions of the Kohn-Sham equation [6] can be used to calculate the surface optical properties within the independent-particle approximation [9]. However, the Kohn-Sham formalism is a ground-state theory. Since the excitation aspect is missing, the resulting optical transition energies are too small [10]. Hedin's GW approximation [11] is the state-of-the-art approach to include the exchange-correlation energy of the excited particles in *ab initio* bandstructure calculations. Apart from a few exceptions, where also the wave functions are updated (see, e.g., Ref. [12]), this is usually done in a perturbative manner, employing the eigenvalues and eigenfunctions from the DFT-LDA calculation as starting point [13]. Calculations of quasiparticle bandstructures in GW approximation have been performed for several semiconductor surfaces with small unit cells [14–16].

[1]) Corresponding author; Phone: +49 3641 947150; Fax: +49 3641 947152;
e-mail: bechsted@ifto.physik.uni-jena.de

 0031-8965/01/18812-1383 $ 17.50+.50/0

During the measurement of optical properties electron–hole pairs are virtually or really excited by the photons in the system. The excited electrons and holes do not only interact with the surrounding electrons, giving rise to the exchange-correlation self-energy. Rather, there is a mutual interaction of the electron and the hole of the pair [17]. The screened attractive interaction gives rise to excitonic effects which can be accompanied by bound electron–hole states (i.e. excitons) in the limit of the effective-mass treatment [18]. The unscreened electron–hole exchange interaction occurring in the two-particle equation [19, 20] can be identified with the local-field effects according to the approach of Adler [21] and Wiser [22] as has been shown in Refs. [23, 24]. The full inclusion of the electron–hole interaction requires the solution of a Bethe-Salpeter equation. This recently became possible for bulk semiconductors [25, 26]. We are aware of only one application for a semiconductor surface, where, however, only some strongly localized surface states needed to be taken into account [27].

In this paper, the progress in including the many-body effects in the calculation of the surface optical properties is discussed. We show that the reflectance anisotropy of complicated surfaces can now be calculated from *first-principles*. Below we describe our methodology. Thereafter the application of the theory is demonstrated for InP(001)2×4 surfaces and the prototypical Si(110) : H face. A brief summary concludes the paper.

2. Method

In order to calculate surface optical spectra we proceed in four steps. First, the energetically favoured surface phase is identified and the equilibrium atomic geometry is determined. The required total-energy calculations are based on the DFT-LDA. The electron–ion interaction is described by nonlocal norm-conserving pseudopotentials [28]. Semi-core states are taken into account by nonlinear core corrections to the exchange and correlation energy. A massively parallel, real-space finite-difference method [29] is used to deal efficiently with the large unit cells needed to describe the surface. A multigrid technique accelerates the convergence. The spacing of the finest grid used to represent the electronic wave functions and charge density is about 10% of a bulk bond length.

The surfaces are modelled by periodic supercells consisting of 12 atomic layers. The material slabs are separated by a vacuum region corresponding to approximately 8 atomic layers. We describe polar surfaces by asymmetric slabs. The atoms in the lowest bilayer are kept frozen and the surface dangling bonds at the bottom layer are satured with pseudohydrogen atoms. We use a linear cutoff function to suppress the signal from the bottom layers in order to avoid spurious effects on the calculated spectra. For Si(110) : H a symmetric slab was used where the atoms in the innermost two atomic layers were kept frozen at the ideal bulk positions. The surface dangling bonds of the Si(110) surface are saturated by hydrogen atoms resulting in a 1×1 translational symmetry. The upper part of the corresponding [110] oriented slab is represented in Fig. 1. The geometries investigated are relaxed until all calculated forces are below 20 meV/Å.

The surface optical property we are interested in here is the reflectance anisotropy for normal incidence. For (001) surfaces the optical anisotropy between the polarization directions $x \equiv [1\bar{1}0]$ and $y \equiv [110]$ is calculated. In case of the (110) surface we identify x and y with the $[1\bar{1}0]$ and [001] directions. The frequency dependent RA can be ob-

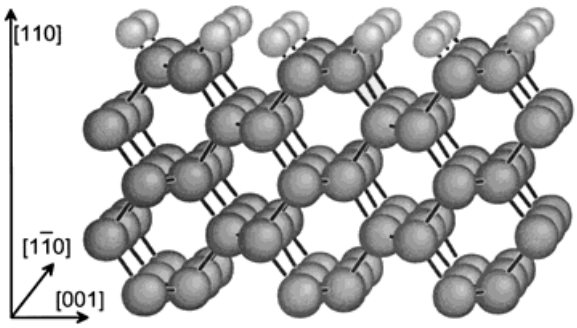

Fig. 1. Upper part of the slab representing the hydrogen-covered Si(110) surface

tained from slab calculations as [4, 32]

$$\frac{\Delta R(\omega)}{R(\omega)} = \frac{4d\omega}{c}\ \mathrm{Im}\ \frac{\alpha_{xx}(\omega) - \alpha_{yy}(\omega)}{\alpha(\omega)}\,, \tag{1}$$

where $\alpha_{ii}(\omega)$ ($i = x$ or y) are the diagonal components of the polarizability tensor of a slab with thickness d and $\alpha(\omega)$ denotes the bulk polarizability. The polarizabilies in Eq. (1) factorize into the polarization function P of the system and matrix elements representing the strength of the optical transitions.

We take advantage of the repeated-slab approximation where the Bloch picture is valid. The wave vector $\mathbf{k}$ within the surface Brillouin zone (SBZ) and the band index n are good quantum numbers. Within the local-density approximation to the exchange and correlation energy the single-particle Kohn-Sham equation yields eigenfunctions $|n\mathbf{k}\rangle$ and eigenvalues $\varepsilon_n(\mathbf{k})$. The polarizability is then given by

$$\begin{aligned}\alpha_{ii}(\omega) = -\frac{2e^2\hbar^2}{V} \sum_{c,v,\mathbf{k}} \sum_{c',v',\mathbf{k}'} \{&M^{i*}_{cv}(\mathbf{k})\, M^{i}_{c'v'}(\mathbf{k}')\, P(cv\mathbf{k}, c'v'\mathbf{k}'; \omega) \\ &+ M^{i}_{cv}(\mathbf{k})\, M^{i*}_{c'v'}(\mathbf{k}')\, P^*(cv\mathbf{k}, c'v'\mathbf{k}'; -\omega)\}\end{aligned} \tag{2}$$

with matrix elements of the velocity operator $\mathbf{v}$

$$M^{i}_{cv}(\mathbf{k}) = \frac{\langle c\mathbf{k}|\, v_i\, |v\mathbf{k}\rangle}{\varepsilon_c(\mathbf{k}) - \varepsilon_v(\mathbf{k})} \tag{3}$$

and V as the volume of the system. In (2) we sum up over pairs of electrons in empty conduction band states $|c\mathbf{k}\rangle$ and holes in occupied valence band states $|v\mathbf{k}\rangle$, that are virtually or really excited by photons. The polarization function P obeys a Bethe-Salpeter equation (BSE) of the form

$$\sum_{c'',v'',\mathbf{k}''} \{H(cv\mathbf{k}, c''v''\mathbf{k}'') - \hbar(\omega + i\Gamma)\delta_{cc''}\delta_{vv''}\delta_{\mathbf{k}\mathbf{k}''}\}\, P(c''v''\mathbf{k}'', c'v'\mathbf{k}'; \omega) = -\delta_{cc'}\delta_{vv'}\delta_{\mathbf{k}\mathbf{k}'} \tag{4}$$

with an effective two-particle Hamiltonian $H(cv\mathbf{k}, c'v'\mathbf{k}')$ and a small damping Γ of the pair excitations.

Within the independent-particle approximation [9] the two-particle Hamiltonian can be directly related to the Kohn-Sham eigenvalues $\varepsilon_n(\mathbf{k})$ of the DFT-LDA,

$$H(cv\mathbf{k}, c'v'\mathbf{k}') = [\varepsilon_c(\mathbf{k}) - \varepsilon_v(\mathbf{k})]\ \delta_{cc'}\delta_{vv'}\delta_{\mathbf{k}\mathbf{k}'}\,. \tag{5}$$

Such diagonal Hamiltonians allow for the immediate calculation of the polarization functions as a second step and, hence, the calculation of the surface optical properties in DFT-LDA quality. By inserting expressions (4) and (5) into the polarizability (2), one obtains the well-known Ehrenreich-Cohen formula.

In the third and fourth step we include the many-body effects in the solution of the BSE. We start with a perturbative treatment of the quasiparticle effects. In first-order perturbation theory only the DFT-LDA eigenvalues are corrected,

$$\varepsilon_n^{\mathrm{QP}}(\mathbf{k}) = \varepsilon_n(\mathbf{k}) + \Delta_n(\mathbf{k}), \tag{6}$$

$$\Delta_n(\mathbf{k}) = \langle n\mathbf{k}|\, \Sigma(\varepsilon_n(\mathbf{k})) - V_{\mathrm{xc}}\, |n\mathbf{k}\rangle\,. \tag{7}$$

The exchange-correlation self-energy operator Σ is taken within the GW approximation [10, 11, 13], whereas V_{xc} represents the local exchange-correlation potential that enters the Kohn-Sham equation. Within the perturbation-theory treatment the Kohn-Sham wave functions are not updated [12]. The two-particle Hamiltonian (5) is modified by the quasiparticle shifts $\Delta_c(\mathbf{k})$ and $\Delta_v(\mathbf{k})$ of electron and hole energies, respectively. The polarization function can again be calculated immediately. Within the resulting independent-quasiparticle approach the same expression as in the independent-particle case holds for the polarizability. Only the spectral properties are changed by the quasiparticle shifts (7).

For surfaces described by slabs containing about 100 atoms many quasiparticle shifts need to be calculated. Therefore, we introduce further approximations and use a model dielectric function and an approximate treatment of the local-field contributions to calculate the screened potential W [33, 34] entering the self-energy operator Σ. This method substantially speeds up the calculations and predicts bulk and surface quasiparticle energies which are within about 0.1 eV of the complete calculations [35, 36]. Even a rather strong variation of the effective dielectric constants induces changes in the energetical positions of surface states of only about 0.1 eV [37].

After real or virtual excitation of electron–hole pairs with photons, the excited electrons and holes do not only interact with the surrounding remaining valence electrons resulting in the renormalization to quasiparticles. Rather, there is a direct interaction of the excited electrons and holes, which is described by the pair Hamiltonian

$$H(cv\mathbf{k}, c'v'\mathbf{k}') = \left[\varepsilon_c^{\mathrm{QP}}(\mathbf{k}) - \varepsilon_v^{\mathrm{QP}}(\mathbf{k})\right] \delta_{cc'}\delta_{vv'}\delta_{\mathbf{kk}'} + W(cv\mathbf{k}, c'v'\mathbf{k}') + \bar{v}(cv\mathbf{k}, c'v'\mathbf{k}') \tag{8}$$

with the matrix elements

$$W(cv\mathbf{k}, c'v'\mathbf{k}') = -\int \mathrm{d}^3\mathbf{x} \int \mathrm{d}^3\mathbf{x}'\, \varphi^*_{c\mathbf{k}}(\mathbf{x})\, \varphi_{c'\mathbf{k}'}(\mathbf{x})\, W(\mathbf{x}, \mathbf{x}')\, \varphi_{v\mathbf{k}}(\mathbf{x}')\, \varphi^*_{v'\mathbf{k}'}(\mathbf{x}') \tag{9}$$

and

$$\bar{v}(cv\mathbf{k}, c'v'\mathbf{k}') = 2 \int \mathrm{d}^3\mathbf{x} \int \mathrm{d}^3\mathbf{x}'\, \varphi^*_{c\mathbf{k}}(\mathbf{x})\, \varphi_{v\mathbf{k}}(\mathbf{x})\, \bar{v}(\mathbf{x} - \mathbf{x}')\, \varphi_{c'\mathbf{k}'}(\mathbf{x}')\, \varphi^*_{v'\mathbf{k}'}(\mathbf{x}') \tag{10}$$

of the (statically) screened Coulomb interaction $W(\mathbf{x}, \mathbf{x}')$ and a bare Coulomb interaction $\bar{v}(\mathbf{x} - \mathbf{x}')$. Only the short-range part of the latter is taken into account in agreement with the physical character of expression (10) as electron–hole exchange. The first contribution (9) (cf. also Fig. 2a) to the total electron–hole interaction includes the classical attraction of electron and hole as represented by the diagonal elements with respect to the Kohn-Sham eigenfunctions $\langle \mathbf{x} \mid n\mathbf{k}\rangle = \varphi_{n\mathbf{k}}(\mathbf{x})$. Because of the long-range character of the electrostatic attraction, this interaction is screened. One has to mention that the

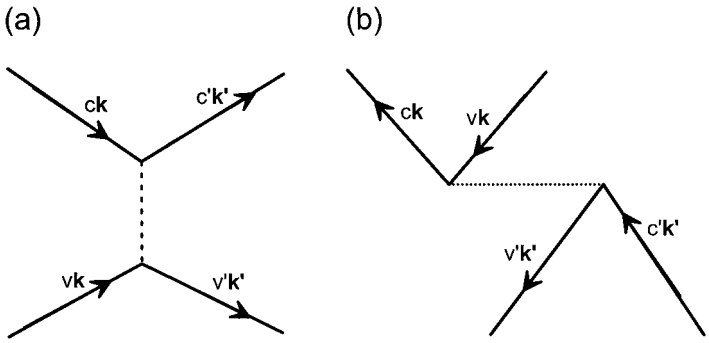

Fig. 2. Schematic representation of a) electron–hole attraction and b) electron–hole exchange. The screened (unscreened) Coulomb interaction is indicated by a dashed (dotted) line

matrix elements of the electron–hole interaction which violate the particle conservation or couple resonant (cv) and nonresonant (vc) pairs have been neglected in expression (8). They are in general small.

The physical meaning of the pair Hamiltonian (8) including the screened electron–hole interaction W is well-known, since it changes over into the Wannier-Mott exciton problem in the effective-mass limit [18]. The interesting point is that the electron–hole exchange term $\sim \bar{v}$ (cf. Fig. 2b) corresponds [23, 24] to the inclusion of local-field effects [21, 22]. Indeed, in the bulk case it has been shown [38] that the BSE (4) gives a polarization corresponding to the macroscopic dielectric function, if the interactions $\sim \bar{v}$ are included.

3. Surface Optical Spectra

3.1 In-rich InP(001)2×4 surface: Quasiparticle effects

We probed a variety of structural models proposed for InP(001) surfaces [7, 39, 40], among them the ζ structure [41] suggested recently to explain cation-rich GaAs(001) surfaces. For slightly P-rich to In-rich conditions we found the β2, α2 and mixed-dimer InP(001)2×4 surfaces to be stable. The accompanying RA spectra change remarkably with the model, i.e., the surface stoichiometry. The β2 model characteristic of slightly P-rich surfaces gives rise to a broad positive RA feature for photon energies between 2.0 and 4.5 eV [30]. With increasing number of In–In surface bonds the RA spectrum develops into a characteristic three-buckle shape. Under the most In-rich conditions the mixed-dimer model (Fig. 3) is stabilized. Its characteristic spectral feature is the development of a pronounced negative RA peak for low photon energies. These findings

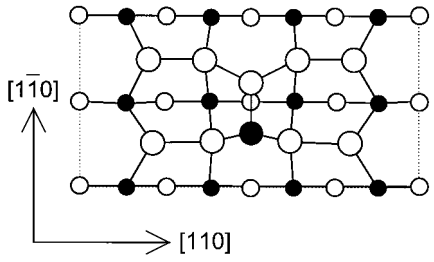

Fig. 3. Top view of the mixed-dimer model of the relaxed InP(001)2 × 4 surface. Empty (filled) circles represent In (P) atoms. Positions in the uppermost two atomic layers are indicated by larger symbols

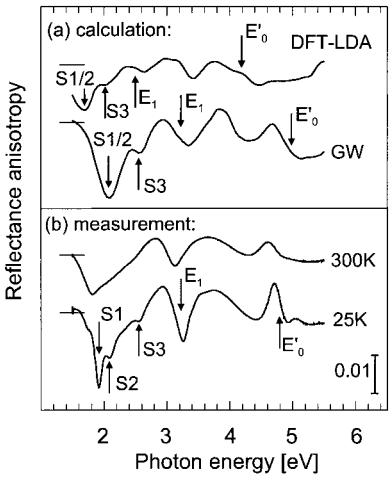

Fig. 4. RA spectra of the In-rich InP(001)2×4 surface. The spectra in the upper panel have been calculated for the mixed-dimer model (Fig. 3) within DFT-LDA and including quasiparticle corrections. The lower panel shows measurements performed at 300 K and 25 K [42]

agree qualitatively with experimental observations [31]. However, the independent-particle theory with the Hamiltonian (5) does neither describe the exact energetical positions of the anisotropy peaks nor their fine structure.

This is demonstrated in Fig. 4. The inclusion of band-index and wave-vector dependent quasiparticle shifts $\Delta_n(\mathbf{k})$ (7) gives rise to a non-uniform blueshift of the entire RA spectrum by about 0.5 eV. Simultaneously, the strength of the positive and negative anisotropies increases and a fine structure appears. The negative anisotropy at low energies splits into peaks at 1.9, 2.1, and 2.6 eV (denoted as S1, S2, and S3). In the high-energy region derivative-like features occur around the energies of the bulk E_1 and E_0' transitions. The calculated spectral behaviour widely agrees with the results of the low-temperature measurement [42]. This holds in particular for the "three-buckle" shape of the RA in the energy region of the E_1 and E_0' transitions. This agreement indicates that sufficiently thick material slabs allow for the description of bulk-related features in the surface optical spectra. The negative anisotropy features originate entirely from the uppermost atomic layers of the slab. Our calculations show that the fine structure with the three minima S1, S2, and S3 in the low-energy region is due to transitions between characteristic surface electronic states [42]. However, the **k**-space sampling (1024 points in the full SBZ) is still not sufficient to allow for the resolution of the S1 and S2 anisotropies in the calculation. But altogether we can conclude that the inclusion of the excitation aspect into the theory via a simplified and numerically efficient algorithm improves considerably the agreement between calculated and measured spectra. This holds for both the peak positions and the peak intensities in the RAS.

3.2 Hydrogenated Si(110) surface: Excitonic effects

The hydrogen-passivated Si(110) surface is a model system for surface optical studies in several aspects. It is one of the first well-defined surface systems that has been studied by RAS [43]. In spectra of surfaces like InP(001)2×4 two types of components of surface optical spectra – "intrinsic" contributions arising from optical transitions within the bulk and "extrinsic" contributions directly related to the surface chemistry [43] – occur. However, since the Si–H bonding and antibonding states give rise to energies far away from the fundamental gap of silicon, only surface-induced bulk-like features occur in the RA spectrum of Si(110):H. Since the RA of passivated Si(110) surfaces is determined by transitions between surface-perturbed bulk states, it does not depend on the details of the surface termination. It has therefore become a calibration standard of RAS apparatus. The RA spectrum of passivated Si(110) surfaces is a textbook example for surface optical properties [44].

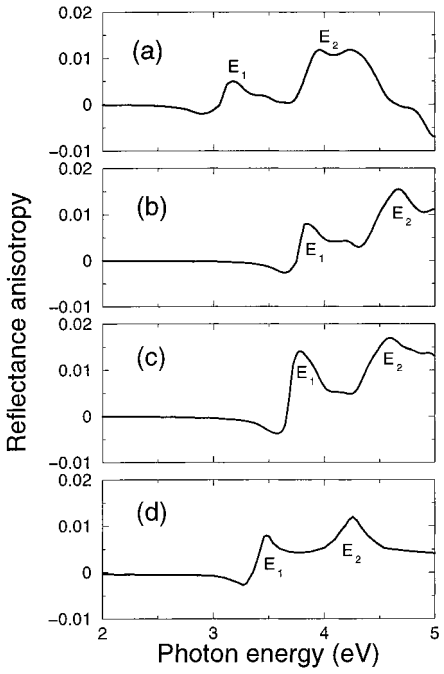

Fig. 5. RA spectra of the H-passivated Si(110)1 × 1 surface. a) Calculated within DFT-LDA. b) Calculated taking quasiparticle shifts into account. c) Calculated including the Coulomb correlation, i.e., screened electron–hole attraction and unscreened electron–hole exchange. d) Measured [45]

Figure 5 presents spectra which have been calculated in different approximations: a) independent-particle approximation using the Hamiltonian (5), b) independent-quasiparticle approximation in which the single-particle energies $\varepsilon_n(\mathbf{k})$ in the Hamiltonian (5) are replaced by the quasiparticle ones $\varepsilon_n^{\mathrm{QP}}(\mathbf{k})$ (6), c) Coulomb-correlated electron–hole pairs with the Hamiltonian (8). The measured data [45] are given in (d). The DFT-LDA spectrum shows two strong positive RA features near the E_1 and E_2 bulk critical point energies. However, the features are far too broad. This is partially due to the use of a too small **k**-point set (140 points) and a slab which is too thin to allow for a complete description of the surface-perturbed bulk wave functions which are responsible for the optical anisotropies in case of Si(110) : H. Denser **k**-point meshs and thicker slabs lead to a much better description of the optical anisotropy at the E_2 energy [46]. They do not improve much the poor representation of the line shape and strength of the anisotropy at the E_1 energy, however. As can be seen from Fig. 5, inclusion of quasiparticle effects leads basically to a blueshift of the spectrum without major changes of the line shape. The intensity of the E_1 peak is still underestimated in comparison with the E_2 structure. This finding is similar to the observation in the absorption spectrum of bulk silicon [9, 25, 26]. Excitonic and, perhaps, local-field effects have to be taken into account.

In principle, this can be done by diagonalizing the Hamilton matrix (8). However, in contrast to surface optical features to which only a few band pairs contribute [27], the rank of the matrix for Si(110) : H becomes very large. The slab contains 24 Si and 4 hydrogen atoms. That means that about 50 valence and 50 conduction bands need to be considered at the 140 **k** points, leading to a number of $N = N_v \cdot N_c \cdot N_k = 350000$ electron–hole pair states. The diagonalization of a matrix with N^2 elements is computationally far too costly. Therefore, we follow an earlier idea by Glutsch et al. [47] to calculate the polarizability from the time evolution of a vector $|\Psi(t)\rangle$ with N elements. In detail, the quantity

$$\sum_{c',v',\mathbf{k}'} M^i_{c'v'}(\mathbf{k}')\, P(cv\mathbf{k}, c'v'\mathbf{k}'; \omega) = \frac{i}{\hbar} \int_0^\infty \mathrm{d}t\, \mathrm{e}^{i(\omega + i\Gamma)\, t}\, \Psi_{cv\mathbf{k}}(t) \tag{11}$$

is calculated. The evolution of the elements of $|\Psi(t)\rangle$ are driven by the pair Hamiltonian

$$\sum_{c',v',\mathbf{k}'} H(cv\mathbf{k}, c'v'\mathbf{k}')\, \Psi_{c'v'\mathbf{k}'}(t) = i\hbar\, \frac{\partial}{\partial t}\, \Psi_{cv\mathbf{k}}(t) \tag{12}$$

with their inital values given by

$$\Psi_{cv\mathbf{k}}(0) = M^i_{cv}(\mathbf{k})\,. \tag{13}$$

We solve the initial-value problem by the central difference ("leap-frog") method where the matrix-vector multiplications $\hat{H}\,|\Psi(t)\rangle$ are distributed on several processors. The upper limit of the Fourier integral in expression (11) can be truncated due to the exponential $e^{-\Gamma t}$. The number of time steps, i.e. the matrix-vector-multiplications, is nearly independent of the dimension of the system. The operation count for this method scales thus quadratically with the dimension of the pair Hamiltonian, N, and is therefore particularly suitable for complex systems as surfaces.

The resulting RA spectrum is presented in Fig. 5c. It contains now in addition to the quasiparticle shifts also the effects of the screened electron–hole attraction and local-field effects (unscreened electron–hole exchange). The most pronounced changes are a distinct increase of the optical anisotropy at the E_1 energy – which is now in much better agreement with experiment – together with a redshift of the entire spectrum by about 0.1–0.2 eV. Including the Coulomb correlation the calculations now also reproduce the negative anisotropy below the E_1 energy. However, there still remain discrepancies between calculation and experiment: The calculated peak positions occur at energies that are about 0.3 eV too high. Our calculations were performed at the theoretical equilibrium lattice constant of 5.378 Å. That leads to an increase of the energy splitting between occupied and empty states by about 0.1 eV compared to calculations at the experimental lattice constant of 5.431 Å. Temperature effects in the measured spectra which are neglected in our calculations result in a redshift of the optical spectra by a similar amount [48]. The remaining difference to the experiment is related to our approximations in calculating the screened Coulomb potential W and to numerical insufficiencies as the relatively small number of $\mathbf{k}$ points. In particular the latter is responsible for the deviation from the measured line shape. That can be seen from DFT-LDA calculations [46] which are computationally far less expensive and can thus be extended to full numerical convergence.

The spectral behaviour of the reflectance anisotropy (1) is a complicated interplay of surface and bulk effects. In order to clarify the origin of the RA features, we present the imaginary parts of the slab polarizabilities in Fig. 6. They exhibit a strong dependence on the light polarization due to the matrix elements (3) which mainly results from modifications of the bulk wave functions due to the truncation of the material. For light polarization parallel to the $[1\bar{1}0]$ direction the E_1 transi-

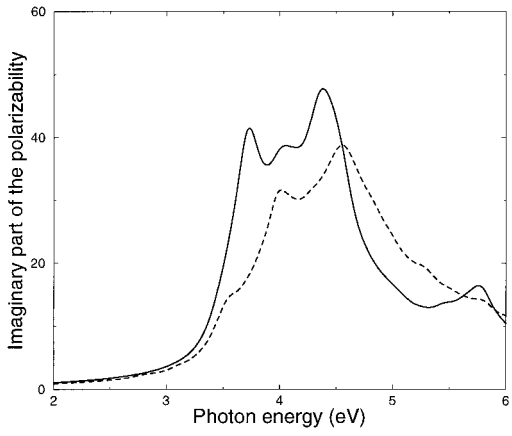

Fig. 6. Imaginary part of the slab polarizability of Si(110):H for two directions of the light polarization. Solid line: $x \,||\, [\bar{1}10]$, dashed line: $y \,||\, [001]$. The calculations were performed including both electron–hole attraction and local-field effects

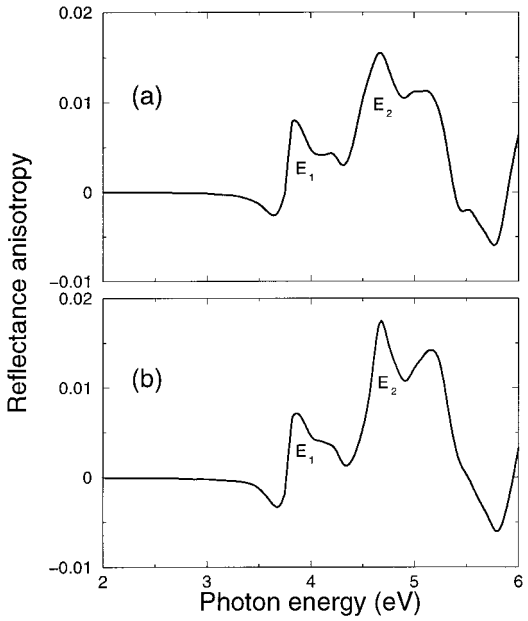

Fig. 7. Comparison of the RAS calculated for Si(110) : H within two approximations: a) independent-quasiparticle approximation, b) electron–hole exchange is included additionally

tions give rise to a strong peak, while there is only a shoulder for the perpendicular polarization. Fig. 6 shows that the negative RA feature below E_1 does not result from the absorption in the surface layers. Rather, it is consequence of the real parts of the slab polarizabilities weighted by the bulk spectrum $\sim \mathrm{Im}\,\frac{1}{\alpha(\omega)}$.

From the calculated spectra in Fig. 5 it is obvious that already an ideal Si(110) : H is characterized by optical anisotropies which correspond to the measured signals. There is no need to assume the existence of surface defects, e.g. of Si and H vacancies as concluded in Ref. [49]. Furthermore, it has been discussed [49] that the surface local-field effect is of particular importance for Si(110) : H surfaces. In order to check that hypothesis we performed additional calculations where we included local-field effects in addition to the self-energy effects. The results are shown in Fig. 7. The figure shows that local-field effects alone lead to rather small changes of the RA spectrum. While we find a distinct influence of local-field effects on the polarizabilities, the effect is nearly cancelled in the RA spectrum. The most important many-body effects, at least for the surface considered, are the renormalization of electrons and holes and their screened Coulomb attraction.

4. Summary

Focusing on the reflectance anisotropy of the In-rich InP(001)2×4 surface and the H-passivated Si(110)1×1 surface we have demonstrated the recent progress in the theoretical description of surface optical properties. The theory is now able to predict optical properties also for surfaces with large reconstructions and with a precision that allows for the identification of specific surface structures. The progress has been made possible by the availability of powerful, massively parallel computers and the development of algorithms which allow for the inclusion of many-body effects in an efficient, yet accurate manner.

Acknowledgements We thank S. Glutsch, L. Reining, and V. Olevano for many helpful discussions. Grants of computer time from the Leibniz-Rechenzentrum München, the John von Neumann-Institut Jülich and the Höchstleistungsrechenzentrum Stuttgart are gratefully acknowledged. The work was partially supported by the EU Research Training Network NANOPHASE (HPRN-CT-2000-00167).

References

[1] W. Richter and J.F. Zettler, Appl. Surf. Sci. **100/101**, 465 (1996).
[2] J.F. McGilp, Prog. Surf. Sci. **49**, 1 (1995).
[3] D.E. Aspnes, Y.C. Chang, A.A. Studna, L.T. Florez, H.H. Farrell, and J.P. Harbinson, Phys. Rev. Lett. **64**, 192 (1990).
[4] R. Del Sole, in: Photonic Probes of Surfaces, Ed. P. Halevi, Elsevier Sci. Publ. Co., Amsterdam 1995.
[5] P. Hohenberg and W. Kohn, Phys. Rev. **136**, B864 (1964).
[6] W. Kohn and L.J. Sham, Phys. Rev. **140**, A1133 (1965).
[7] W.G. Schmidt and F. Bechstedt, Surf. Sci. **409**, 474 (1998).
[8] F. Bechstedt, A. Stekolnikov, J. Furthmller, and P. Käckell, Phys. Rev. Lett. **87**, 016103 (2001).
[9] B. Adolph, V.I. Gavrilenko, K. Tenelsen, F. Bechstedt, and R. Del Sole, Phys. Rev. B **53**, 9797 (1996).
[10] F. Bechstedt, Adv. Solid State Phys. **32**, 161 (1992).
[11] L. Hedin, Phys. Rev. **139**, A796 (1965).
[12] O. Pulci, F. Bechstedt, G. Onida, R. Del Sole, and L. Reining, Phys. Rev. B **60**, 16758 (1999).
[13] R.W. Godby, M. Schlüter, and L.J. Sham, Phys. Rev. B **37**, 10159 (1988).
[14] X. Zhu, S.B. Zhang, S.G. Louie, and M.L. Cohen, Phys. Rev. Lett. **63**, 2112 (1989).
[15] J.E. Northrup, M.S. Hybertsen, and S.G. Louie, Phys. Rev. Lett. **66**, 500 (1991).
[16] M. Rohlfing, P. Krüger, and J. Pollmann, Phys. Rev. B **48**, 17791 (1993).
[17] M. Rohlfing and S.G. Louie, Phys. Rev. B **62**, 4927 (2000).
[18] G.D. Mahan, Many-Particle Physics, Plenum Press, New York 1990.
[19] L.J. Sham and T.M. Rice, Phys. Rev. **144**, 708 (1966).
[20] W. Hanke and L.J. Sham, Phys. Rev. Lett. **43**, 387 (1979); Phys. Rev. B **21**, 4656 (1980).
[21] S. Adler, Phys. Rev. **126**, 413 (1962).
[22] N. Wiser, Phys. Rev. **129**, 62 (1963).
[23] W. Hanke and L.J. Sham, Phys. Rev. B **12**, 4501 (1975).
[24] R. Del Sole and E. Fiorino, Phys. Rev. B **29**, 4631 (1984).
[25] S. Albrecht, L. Reining, R. Del Sole, and G. Onida, Phys. Rev. Lett. **80**, 4510 (1998).
[26] L.X. Benedict, E.L. Shirley, and R.B. Bohn, Phys. Rev. Lett. **80**, 4514 (1998).
[27] M. Rohlfing and S.G. Louie, Phys. Rev. Lett. **83**, 856 (1999).
[28] M. Fuchs and M. Scheffler, Comput. Phys. Commun. **119**, 67 (1999).
[29] E.L. Briggs, D.J. Sullivan, and J. Bernholc, Phys. Rev. B **54**, 14362 (1996).
[30] F. Bechstedt, O. Pulci, and W.G. Schmidt, phys. stat. sol (a) **175**, 5 (1999).
[31] K.B. Ozanyan, P.J. Parbrook, M. Hopkinson, C.R. Whitehouse, Z. Sobiesierski, and D.I. Westwood, Appl. Phys. **82**, 474 (1997).
[32] F. Manghi, R. Del Sole, A. Selloni, and E. Molinari, Phys. Rev. B **41**, 9935 (1990).
[33] F. Bechstedt, R. Del Sole, G. Cappellini, and L. Reining, Solid State Commun. **84**, 765 (1992).
[34] G. Cappellini, R. Del Sole, L. Reining and F. Bechstedt, Phys. Rev. B **47**, 9882 (1993).
[35] B. Wenzien, P. Käckell, F. Bechstedt, and G. Cappellini, Phys. Rev. B **52**, 10897 (1995).
[36] W.G. Schmidt, J.L. Fattebert, J. Bernholc, and F. Bechstedt, Surf. Rev. Lett. **6**, 1159 (1999).
[37] J.E. Northrup, Phys. Rev. B **47**, 10032 (1993).
[38] P. Hahn, Diploma thesis, Friedrich-Schiller-Universität Jena, 2001.
[39] O. Pulci, K. Lüdge, W.G. Schmidt, and F. Bechstedt, Surf. Sci. **464**, 272 (2000).
[40] W.G. Schmidt, Appl. Phys. A accepted.
[41] S.-H. Lee, W. Moritz, and M. Scheffler, Phys. Rev. Lett. **85**, 3890 (2000).
[42] W.G. Schmidt, N. Esser, A.M. Frisch, P. Vogt, J. Bernholc, F. Bechstedt, M. Zorn, T. Hannappel, S. Visbek, and W. Richter, Phys. Rev. B **61**, R16335 (2000).
[43] D.E. Aspnes and A.A. Studna, Phys. Rev. Lett. **54**, 1956 (1985).
[44] P.Y. Yu and M. Cardona, Fundamentals of Semiconductors, Springer-Verlag, Berlin 1999.
[45] T. Yasuda, D.E. Aspnes, D.R. Lee, C.H. Bjorkman, and G. Lucovsky, J. Vac. Sci. Technol. A **12**, 1152 (1994).
[46] W.G. Schmidt and J. Bernholc, Phys. Rev. B **61**, 7604 (2000).
[47] S. Glutsch, D.S. Chemla, and F. Bechstedt, Phys. Rev. B **54**, 11592 (1996).
[48] P. Lautenschlager, M. Garriga, L. Viña, and M. Cardona, Phys. Rev. B **36**, 4821 (1987).
[49] B.S. Mendoza, R. Del Sole, and A.I. Shkrebtii, Phys. Rev. B **57**, R12709 (1998).